Materials Research. 2022; 25:e20220315
DOI: https://doi.org/10.1590/1980-5373-MR-2022-0315

Low Cycle Fatigue Behavior of Al-Mg-Si Alloys Extruded Parts

D.F.L. Nascimento[a], A.M.B. da Silva-Antunes[b], M. Paes[c*], C.A.R.P. Baptista[b]

[a]Faculdade de Tecnologia de Cruzeiro Prof. Waldomiro May, FATEC/CP, Cruzeiro, SP, Brasil.
[b]Universidade de São Paulo, Escola de Engenharia de Lorena, Departamento de Engenharia de Materiais, Lorena, SP, Brasil.
[c]Universidade de São Paulo, Escola de Engenharia de São Carlos, Departamento de Engenharia de Materiais, São Carlos, SP, Brasil.

Received: July 12, 2022; Revised: September 22, 2022; Accepted: October 06, 2022

Over the past years, Al-Mg-Si alloys have been largely applied in automotive industry, which has required a deep knowledge of their mechanical properties and the influence of precipitates distribution on their mechanical behavior. This work evaluated the main mechanical properties of AA6005, AA6063, and AA6351 alloys by means of tensile and low cycle fatigue tests with 0.005 seg^{-1} deformation rate and 0.3% < ε_{at} <1.2% strain amplitudes. Besides, the hysteresis loop and internal stress analysis were investigated to analyze hardening and softening phenomena and to evaluate the friction and back stresses, respectively. Macro and microstructural were performed focusing in intermetallic distribution. Concerning the low cycle fatigue behavior, AA6351 presented shorter lives for strain amplitudes higher than 0.5%, and AA6005 showed the highest fatigue strength and fatigue ductility. AA6063 showed the lowest fatigue strength due to the presence of coarse particles (Fe,Mn)SiAl. During internal stress analysis, the highest value of friction stress for AA6351 indicates the effect of hardener precipitates are the most relevant role for cyclic loadings and the lowest back-to-friction stress ratio indicating that deformation is controlled by particles. In the other hand, AA6063 showed the lowest friction stress due to low amount of fine precipitates.

Keywords*: Al-Mg-Si alloys, low cycle fatigue, internal stress, cyclic hardening, cyclic softening.*

1. Introduction

Al-Mg-Si alloys (AA6XXX series) are some of the most important, widely used precipitation-hardenable aluminum materials. The amount of silicon in Al-alloys can influence the stoichiometry of Mg_2Si and α-(Fe,Mn)SiAl, which are the main precipitates affecting fatigue behavior[1]. In these alloys, a few elements (e.g., Mn and Cr) are used for grain control, and silicon in high percentage can be segregated to grain boundaries, causing fracture of the boundary during recrystallization1[2,3]. The mechanical properties of aluminum alloys depend on the interaction among chemical composition, microstructure, heat treatment, and strain processes, in which dislocations and alloy elements are the most significant factors for the hardening phenomena. The presence of particles creates a barrier to dislocations movement, thus influencing the hardening rate and the slope of the stress-strain curve[1].

Some of the aspects that control the main mechanical properties in the Al-Mg-Si alloys are:

Intermetallic coarse particles shaped mainly during solidification and containing Fe and Si. They include insoluble compounds such as Fe, Mn(Al_6), Fe(Al_3), and α-Al(Fe, Mn) Si and others partially soluble (e.g., Mg_2Si)[4].

Dispersoids, which are intermetallic compounds containing Cr, Mn, and Zr.

Fine precipitates shaped during heat treatment, which promote hardening, yield, and tensile strength increase.

Grain size and shape after recrystallization, which, under the influence of dynamic recovery due to the high stacking fault energy (SFE) of aluminum, are significant to microstructural features.

Dislocation structures, which are important for the hardening process due to interaction with intermetallic and dispersoid particles.

In terms of mechanical properties, intermetallic coarse particles do not influence yield and tensile strength significantly; however, they reduce the alloys ductility. On the other hand, the fine precipitates increase both yield and tensile strength and can act as crack nucleation sites during the fatigue process[5]. Crack nucleation during cyclic loading also occurs due to the presence of Mg_2Si in the grain boundaries, leading to a tensile concentration in those points[6]. According to TEM analysis performed by Jiang et al.[7], the presence of Mg_2Si particles anchors the dislocations movement creating high-energy points and favoring the crack nucleation. Considering the techniques available for fatigue life prediction the strain-life study conducts to a general law that take into account the high cycle and low cycle fatigue approaches. This approach considers the total deformation amplitude ε_{at} observed in the hysteresis loop as

*e-mail: marcelo.paes@usp.br

being a summation of ε_{ae} (elastic component) and ε_{ap} (plastic component) according to Equation 1:

$$\varepsilon_{at} = \varepsilon_{ae} + \varepsilon_{ap} \quad (1)$$

The cyclic stress strain curves (CSSC) are very useful to evaluate the cyclic hardening and softening of the alloy. The multiple hysteresis loop in distinct strain amplitudes and gathering to CSSC can be described in Equation 2:

$$\varepsilon_{at} = \frac{\sigma_a}{E} + \left(\frac{\sigma_a}{K'}\right)^{\frac{1}{n'}} \quad (2)$$

Where E is the Young's modulus, *K'* is the cyclic strength coefficient and *n'* is the cyclic hardening exponent[8]. Considering the Basquin and Coffin Manson´s relationships for, respectively, stress-life and strain-life fatigue, the general equation for low cycle fatigue behavior, can be written as Equation 3:

$$\varepsilon_{at} = \frac{\sigma'_f}{E}(2Nf)^b + \varepsilon'_f (2Nf)^c \quad (3)$$

Where E is the Young's modulus, $2Nf$ is the number of reversals to failure, σ'_f and ε'_f are the fatigue strength and ductility coefficients b, and *c*, are the fatigue strength and ductility exponents, respectively[9].

Other studies involving Al-Mg-Si alloys confirms the hardening/softening phenomena during cyclic strain control tests and relating that to microstructural approach[10].

During the study of cyclic stress-strain behavior the cyclic softening and hardening processes are expressed by the change in the stress amplitude necessary to cause a given strain amplitude. The applied stress must be in equilibrium with internal stresses, which can be considered in terms of the distance in which they are effective. The concept of internal stresses appears both in visco-plastic models of continuum mechanics and microscopic theories of deformation[11]. Two internal stress parameters obtained directly from the hysteresis loop, namely the friction stress and the back stress, are often used in the study of the cyclic behavior of metallic materials. The friction stress σ_f is the stress required locally for a dislocation to move and is mainly related with short-range obstacles such as the lattice friction. The back stress σ_b provides a long-range interaction with mobile dislocations and is mainly related to the microstructural barriers or strain incompatibilities in the material[12]. In metallurgical terminology, this refers to the stress that arises against the dislocation movement due to the stacking of same signal dislocations. Being of elastic nature, the back stress decreases during the reversed deformation and then increases again in the opposite direction, in order to resist the continuity of deformation[13,14]. Therefore, internal stresses are defined based on dislocation behavior during plastic deformation and are empirically related to the microstructural quantities, such as grain size and dislocation density.

These two internal stresses (back and friction stress) are determined according to Cottrell method as Figure 1 below, where σ_p is the peak stress.

According to Giordana et al.[15] , Meininger and Gibeling[16], the internal stresses can be defined as below:

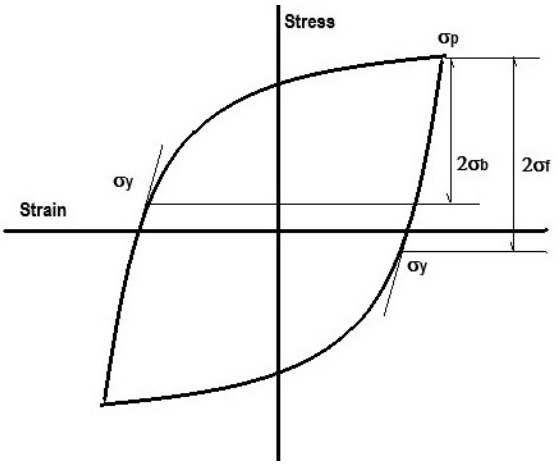

Figure 1. Cottrell method to internal stresses.

$$\sigma_f = \frac{\sigma_p + \sigma_y}{2} \quad (4)$$

$$\sigma_b = \frac{\sigma_p - \sigma_y}{2} \quad (5)$$

Proudhon et al.[17], observed in AA6111 alloy the effects of precipitates distribution in internal stress. The back stress is small in cases of high precipitates volume fraction favoring the friction stress domain. Thus, the friction stress prevails. Other features that consider the evolution of back stress could also be observed using different alloys[12] as the internal stress evolution with the number of cycles indicating the strain hardening/softening phenomena[18].

The aim of this work is to assess three Al-Si-Mg alloys in terms of their low cycle fatigue behavior by means of strain-controlled tests and considering tensile tests to determine their main mechanical properties. The relationship between fatigue properties, internal stresses, microstructure and hardening precipitates is discussed in order to characterize the cyclic deformation mechanisms. Besides, a fractographic analysis is necessary to correlate crack propagation rate and microstructure.

2. Materials and Methods

The materials used in this work were AA6005, AA6063, and AA6351 alloys in T6 temper, received as 10 mm diameter bars, solution treated at 580ºC and aged at 180ºC for 6 hours. Samples were machined as per ASTM E8/E8M-13[19] and E606/E606M-21[20] for tensile and low cycle fatigue tests, respectively. These samples were produced by direct extrusion in which the billets are heated in a furnace until complete solubilization of secondary phases. Once at the temperature is reached a portion of lubricant is applied to the billet and ram to maintain them together. After that, a pressure is applied to the billet that is forced to move through a die. Thus, the metal is squeezed through the die and exit the extrusion press.

Tensile tests samples were machined with gage length of 30 mm, length of reduced section of 32 mm, length of grip

section of 40 mm, radius of fillet of 6 mm, gage diameter of 6 mm and diameter of grip section of 9 mm.

Fatigue test samples were machine gage length of 8 mm, length of reduced section of 21.08 mm, length of grip section of 49 mm, radius of fillet of 12 mm, gage diameter of 5 mm and diameter of grip section of 8 mm.

Table 1 shows the chemical composition of the alloys according to ASTM B221-21[21] and the verified composition by using a spectrophotometer Ametek Spectromaxx LMF05.

Macro and microstructural characterization of longitudinally sectioned extruded bar samples were performed. For the sample preparation, the sequence of sandpapers 600, 800, 1200 and 2000 was adopted, followed by final polishing with colloidal silica suspension. Samples were etched with 0.5% HF solution and the macrostructure was taken under polarized light. The samples were analyzed using an Olympus BX51M optical microscope and a LEO 1450VP scanning electron microscope, and the volumetric fraction of particles was determined by means of Image J software.

Tensile tests were performed for each alloy in a MTS 810.23M equipment, according to ASTM E8/E8M-13[19] at 1.0 mm/min speed and with a 25 mm extensometer as reference.

Low cycle fatigue tests were conducted at 0.005 seg^{-1} deformation rate and $0.3\% < \varepsilon_{at} < 1.2\%$ strain amplitudes with triangular wave shape. The peaks of true stress-strain hysteresis loops from different deformation amplitudes provided the cyclic stress-strain curves, and the elastic and plastic deformation amplitudes determined from the half-life hysteresis loops were used to calculate the strain-life curve parameters according to Equation 3.

Internal stress analysis was performed in order to evaluate the friction and back stresses σ_f and σ_b whose calculation was performed in accordance to the technique proposed by Kuhlmann-Wilsdorf and Laird[13] based on the method initially suggested by Xu et al.[12], Bai et al.[18], Cottrell[22]. Considering the peak stress (σ_p) as the stress amplitude in the loading cycle and denoting the flow stress by σ_y, see Figure 1, the friction and back stresses were estimated by Equations 1, 2 and 3[16]. The internal stress evolution was determined, for each alloy, taking the recorded hysteresis loops for the 0.5% strain amplitude tests.

3. Results

The results were summarized into four sections, namely microstructural analysis, tensile properties, low cycle fatigue tests, and fracture surface analysis.

3.1. Macro and Microstructural analysis

Figures 2 and 3 shows the alloys macro and microstructure, respectively. Figure 2 shows green and yellow vertical lines in the edges that bounds the machined diameter used in specimens for tensile and fatigue tests. Figures 2a and b display the recrystallized grains in the edges and elongated and coarse grains in the center of, respectively, AA6005 and AA6351 samples. Figure 2c shows a totally recrystallized structure mainly due to the low volume fraction of particles rich in manganese that enables recrystallization. Moreover, the low amount of manganese in AA6063 avoids the occurrence of pinning in the grain boundaries, thus leading to recrystallization[23].

Figures 3a and b show the microstructure of AA6005 alloy and (c) and (d) depict that of AA6351. Coarse intermetallic particles of α-(Fe,Mn)SiAl of 3μm maximum size for AA6005 and 5μm maximum size for AA6351 can be observed. Figures 3e and f show the microstructure of AA6063 with oblong particles of 8μm α-FeSiAl. The coarse particles observed under optical microscope are not the hardening ones generated during aging, but insoluble particles that fracture during mechanical processes and produce voids whose coalescence reduces the shear energy.

3.2. Tensile properties

Figure 4 depicts the tensile stress-strain curves for AA6005, AA6063, and AA6351 alloys and Table 2 shows their main mechanical properties containing both mean and standard deviations for each property, where σ_{ys} is the yield strength, σ_{uts} is the ultimate tensile strength, ΔL is the elongation in percentage, E is Young's modulus.

The results in Table 2 show the AA6351 has the highest σ_{ys} and σ_{uts} values, which, according to Table 1, can be related to the higher Si and Mn content of this alloy. It is known that a manganese addition from 0.5% increases both yield strength and ultimate tensile strength with no ductility influence[24]. In terms of microstructure, the manganese addition creates $MnAl_6$ dispersoids, which hampers the dislocations movement and hardens the material[25]. On the other hand, the low amount of manganese in AA6063 justifies its lower yield and tensile strength. AA6005 alloy, showed intermediate mechanical properties between AA6063 and AA6351 alloys. The amount of manganese in AA6005 alloy is higher than AA6063 that justifies both σ_{uts} and σ_{ys}.

Table 1. Chemical composition of aluminum alloys according to ASTM B221-21[21] specification and verified.

Alloy	Si	Fe	Cu	Mn	Mg	Cr	Zn	Ti
AA6005 Specified	0.50-0.90	0.35 max	0.30 max	0.50 max	0.40-0.70	0.30 max	0.20 max	0.10 max
AA6005 Verified	0,82	0,22	0,09	0,25	0,47	0,002	<0,001	0,03
AA6063 Specified	0.20-0.60	0.35 max	0.10 max	0.10 max	0.45-0.92	0.10 max	0.10 max	0.10 max
AA6063 Verified	0,53	0,18	0,01	0,02	0,44	0,001	0,001	0,03
AA6351 Specified	0.70-1.30	0.50 max	0.10 max	0.40-0.80	0.40-0.80	-	0.20 max	0.20 max
AA6351 Verified	1,01	0,19	0,10	0,48	0,37	-	0,001	0,03

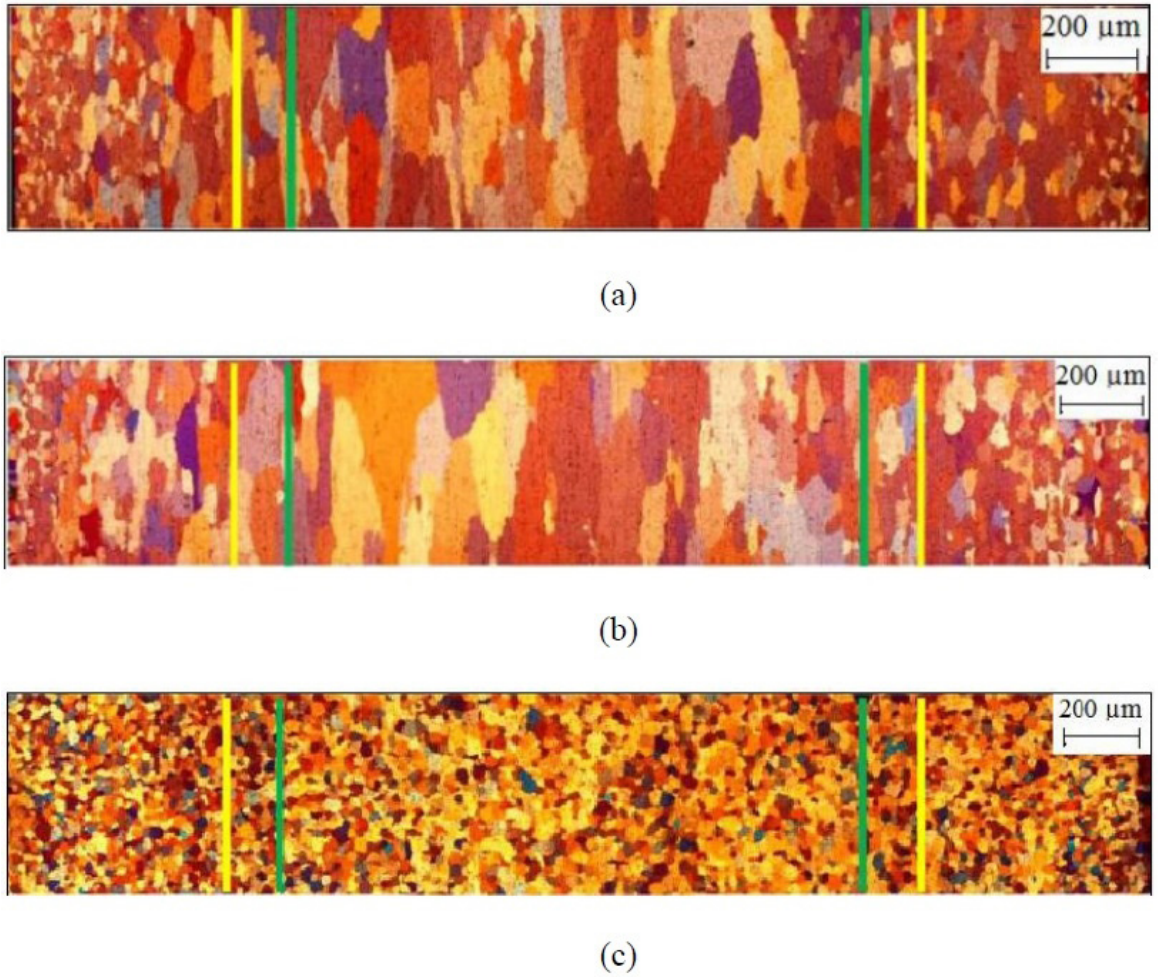

Figure 2. Macrostructure of AA6005 (a), AA6351 (b), and AA6063 (c). 37,5X Magnification.

Table 2. Mechanical properties of the studied aluminum alloys.

Alloy	σ_y (MPa)	σ_{uts} (MPa)	ΔL (%)	E (GPa)	σ_{uts} / σ_y
AA6005	256±0.97	286±1.11	18±0.59	66±1.55	1.12±0.01
AA6063	230±0.54	261±0.86	19±0.62	63±0.72	1.14±0.00
AA6351	331±2.58	354±2.46	15±0.45	68±1.54	1.07±0.00

Yet, AA6351 shows the highest Young's modulus (E) value, compared to AA6005 and AA6063, indicating its higher elastic stiffness. Regarding the elongation (ΔL), AA6005 and AA6063 show higher values associated with low values of yield strength and tensile strength.

The σ_{uts}/σ_{ys} ratio shows the material strain-hardening grade, for which values above 1.4 is considered high, whereas those below 1.2 are considered low[8]. In this study, the ratio was below 1.2 for all aluminum alloys, revealing a high SFE for the materials where the narrow distance between partial dislocations enables cross slip and further dislocation extinction, thus hampering the occurrence of strain-hardening.

Towards a better comprehension of strain hardening, true-stress x true-strain tests determined the strain-hardening exponent (*n*) and Ludwik model was applied. The strain-hardening exponent (*n*) is a material's capacity for hardening during plastic strain, *K* is the strength coefficient, and E is the elasticity modulus. Although *K* and *n* are considered constants, they also depend on processing conditions. The higher the *n,* the higher the curve inclination, and the lower the *n*, the closer the curve to a horizontal shape.

Table 3 shows *K* and *n* calculated by Ludwik model.

Low values of *n* were observed (<0.1) for the alloys tested due to the high SFE in aluminum alloys, AA6351 showed the highest *K* value, according to the high σ_{uts} and σ_y, and AA6063 showed the highest *n*, as depicted in the σ_{uts}/σ_y ratio.

3.2.1. Effect of intermetallic phases on tensile properties

In a nutshell, it is possible to summarize the effects of alloy elements and intermetallic phases in main mechanical

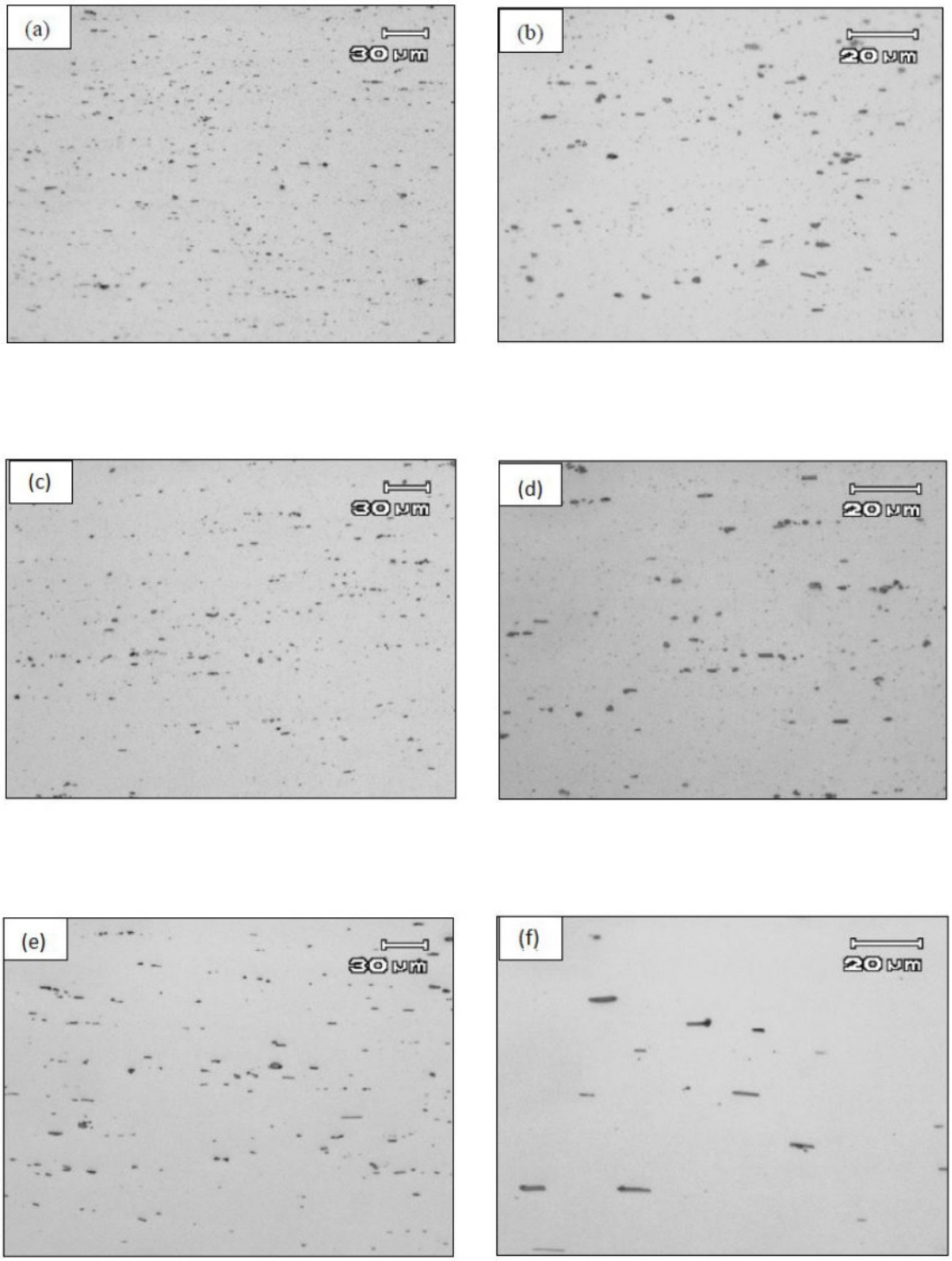

Figure 3. Microstructures of AA6005 alloy under (a) 200× magnification, (b) 500×, AA6351 alloy (c) 200×, (d) 500× and AA6063 alloy (e) 200×, (f) 500× in as-cast and T6 temper conditions.

Table 3. *K* and *n* for true-strain x true-stress tests.

Alloy	*K* (MPa)	*n*
AA6005	382±2.64	0.087±0.002
AA6063	358±4.04	0.096±0.003
AA6351	451±3.78	0.067±0.001

properties during tensile test according to Table 4. It depicts the influence of elements and compounds on mechanical properties by upward and downward arrows, e. g. manganese addition, increases (↑) σ_{uts} justified by line named "Causes". The discussion of results, were discussed in the previous topic.

Table 4. Elements and intermetallic phases effects.

Element	σ_{uts} (MPa)	σ_y (MPa)	σ_{uts}/σ_y	*K* (MPa)	*n*
Mn addition	↑	↑	↓	↑	↓
Si addition	↑	↑	↓	↑	-
$MnAl_6$	↑	↑	-	↑	↓
Cause	*Alloying element effect and hampering of dislocations by $MnAl_6$.*	*Alloying element effect and hampering of dislocations by $MnAl_6$*	*Low strain hardening (<1.2). Due to high SFE.*	*Alloying element effect and hampering of dislocations by $MnAl_6$*	*All hardening exponent <0,1. Due to high SFE.*

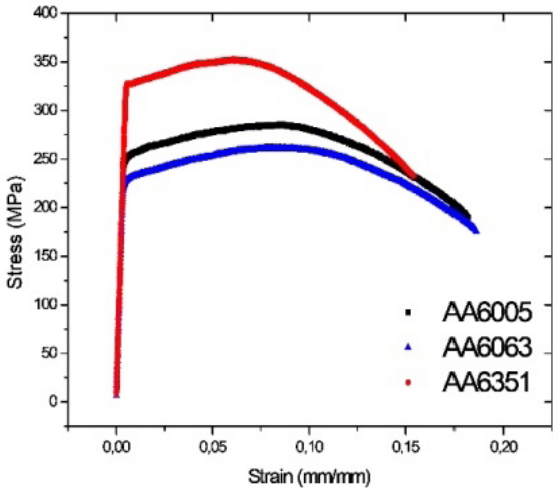

Figure 4. Stress-strain curves for the three Al-Mg-Si alloys.

Table 5. Properties of cyclic stress-strain curves.

Alloy	*K'* (MPa)	*n'*
AA6005	440	0.096
AA6063	354	0.072
AA6351	733	0.162

3.3. Low cycle fatigue analysis

Figure 5 shows the peak stress (σ_p) evolution with the number of deformation cycles under strain control for six different % ε_{at} (total strain amplitude) values. For all alloys tested the cyclic stress response is mainly characterized by slight hardening followed by a variable softening, it means that the peak stress is strongly dependent on the applied strain amplitude from 0,5 to 1,2%[12,24]. It was an expected behavior due to high SFE of aluminum that presents high dislocations mobility favoring the cross slip and consequently softening the material. Mrówka-Nowotnik & Sieniawsky[24] and Borrego et al.[26], reported a similar behavior as aforementioned and observed a short cyclic hardening followed by a long cyclic softening for AA6XXX alloys.

Figure 6 shows the stabilized half-life hysteresis loops for different strain amplitudes, translated to a common point. The Masing behavior is closer to an ideal shape only for AA6351. The aforementioned behavior was observed in alloys hardenable by precipitation whose distance between precipitates is small and non-shearable, promoting a strain control by such precipitates. On the other hand, a large distance between particles leads to a non-Masing behavior, in which the strain is controlled by the aluminum matrix[26].

Table 5 shows the properties of cyclic stress-strain curves, where the strain hardening mechanism seems to change during cyclic loading. Differently from the results in Table 3, AA6351 shows the highest cyclic strain hardening exponent (n'), followed by AA6005 and AA6063. Both size and distance between precipitated particles may be the cause for such behavior reversal in terms of *n*' and, during cyclic loading, the hardening effect seems to be deeply affected by the interaction between dislocation and intermetallic particles (Fe, Mn)SiAl, and Mg_2Si).

The *low cycle fatigue properties* were determined by a linear fit of *log* (ε_a) versus *log(2N$_f$)* obtained for each test by the least square method. Figure 7 depicts the low cycle fatigue curves and Table 6 shows the low cycle fatigue properties.

The transition life that bounds the low cycle to a high cycle state is 500<2Nf<700 for AA6005 and AA6063 and 2Nf<200 for AA6351. During low cycle behavior, in which *2Nf* is lower than 1000 reversals, AA6351 shows fatigue life lower than those of the other alloys, mainly due to its low ductility. However, as the strain amplitude decreases, the fatigue life increases for AA6351.

As shown in Table 2, AA6351 has a low σ_{uts}/σ_y ratio, and a low strain-hardening exponent, thus implying in higher tolerance to fatigue damage and avoidance of a catastrophic crack propagation. On the other hand, AA6063 shows lower strain-hardening exponent, σ_{uts}/σ_y ratio higher than those of other alloys, and lowest fatigue life for low strain amplitudes.

Table 6 shows the low cycle fatigue properties, where σ'_f is the fatigue strength coefficient, *b* is the fatigue strength exponent, ε'_f is the fatigue ductility coefficient, and *c* is the fatigue ductility exponent.

AA6005 showed the highest fatigue strength coefficient (σ'_f) and the highest fatigue ductility coefficient (ε'_f) and, according to Figure 7d, the most satisfactory behavior for different strain amplitudes, except for situations in which the reversals to failures are higher than 1000 cycles.

Christ & Mughrabi[27], Liu et al.[28] and Brammer et al.[29], claimed the cycle strain-stress path is highly influenced by the material's microstructure and intermetallic particles. Both damage grade and rate are controlled by the matrix strength and size, morphology, and distribution of intermetallic phases. A few samples in AA6063 showed an abrupt total fracture

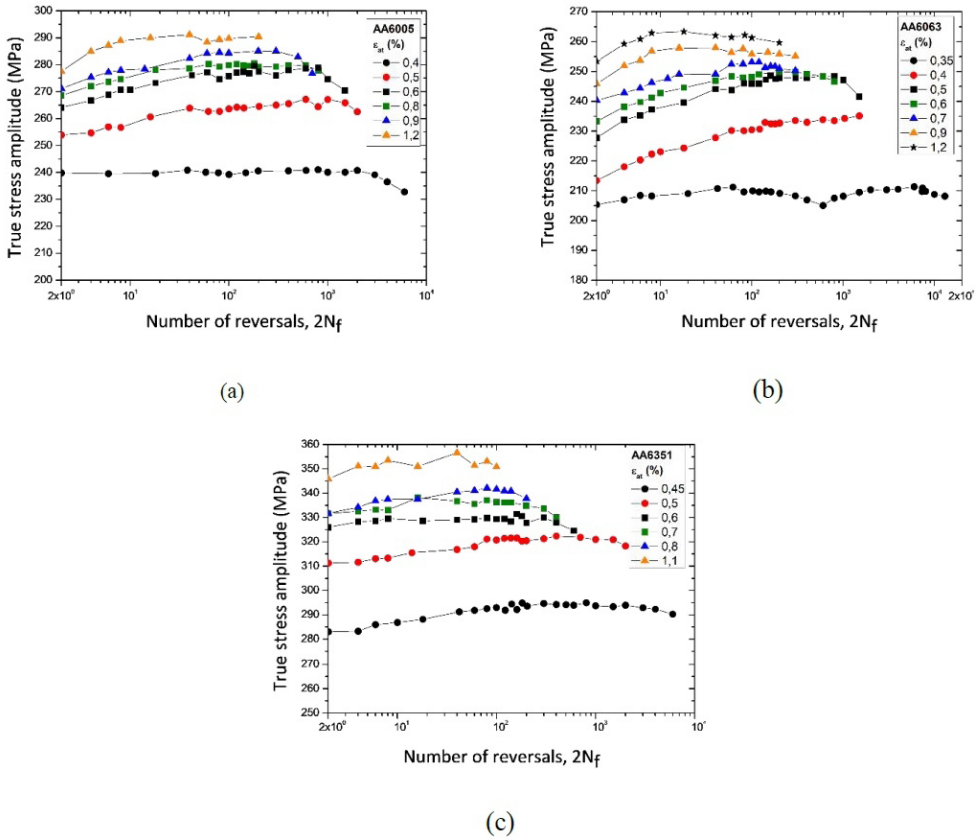

Figure 5. Evolution of peak stress of aluminum alloys under low cycle fatigue. (a) AA6005, (b) AA6063, and (c) AA6351.

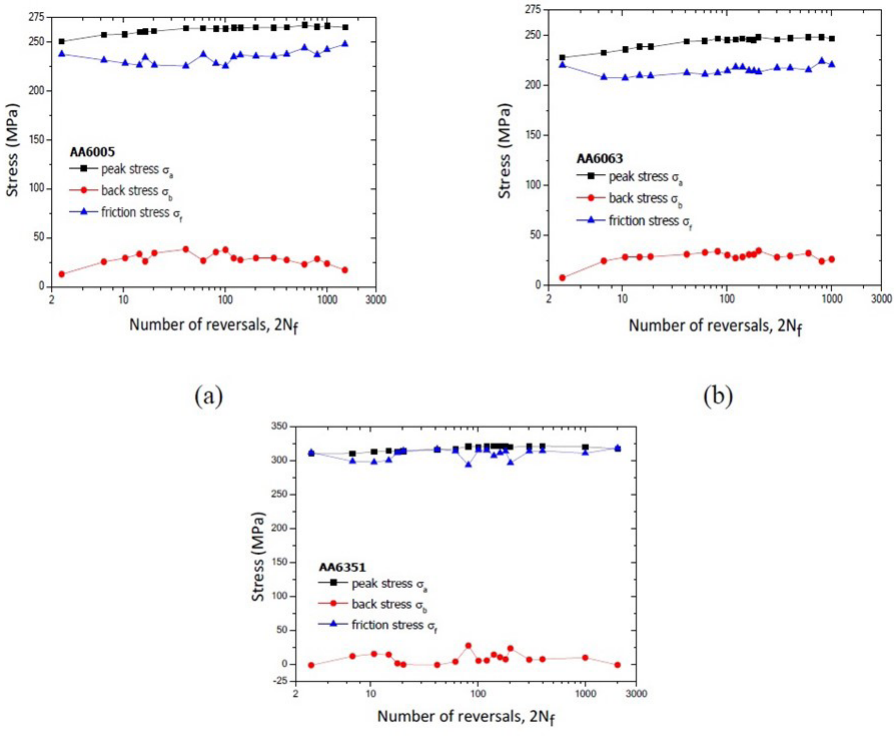

Figure 6. Steady-state hysteresis loops, translated to a common point, for aluminum alloys: (a) AA6005, (b) AA6063, and (c) AA6351.

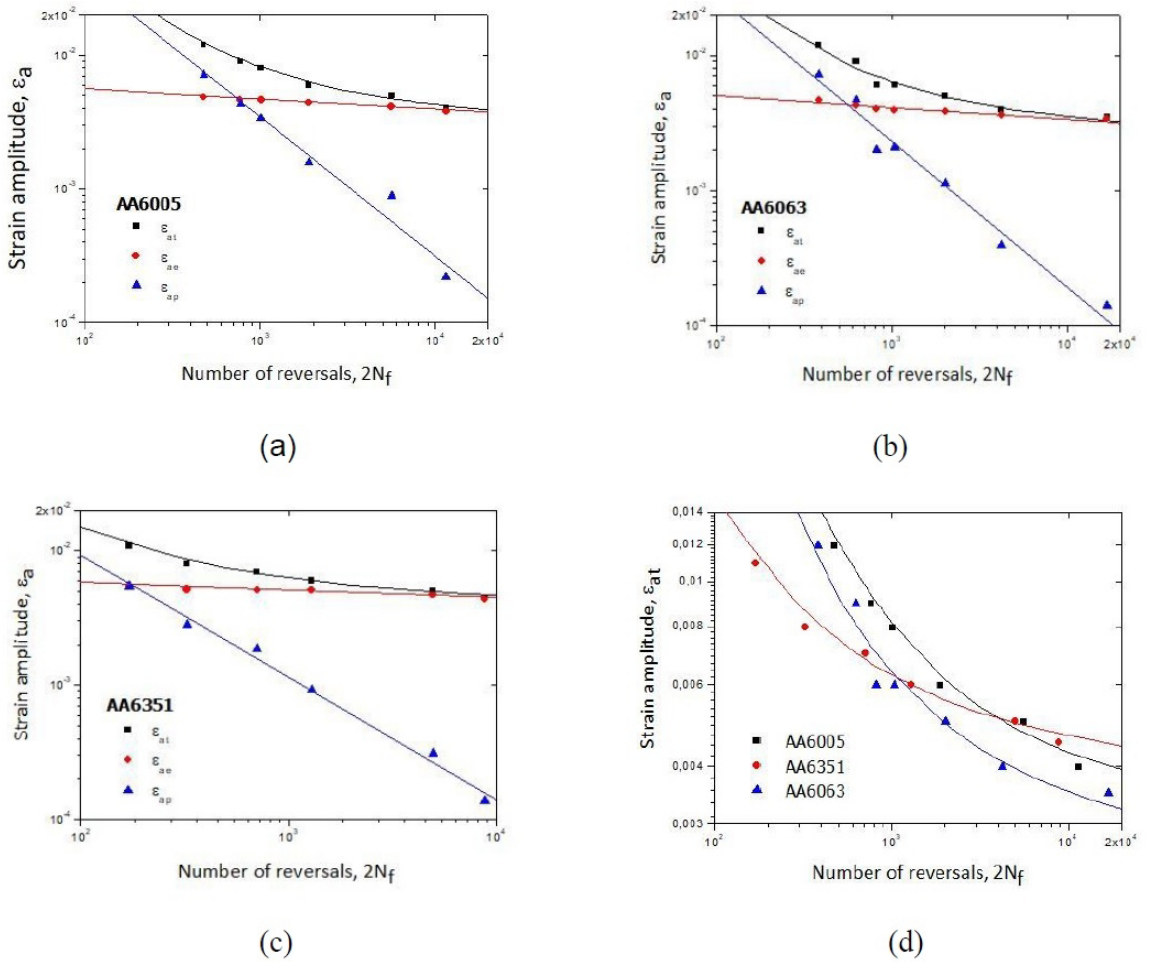

Figure 7. Low cycle fatigue curves. (a) AA6005, (b) AA6063, (c) AA6351, and (d) Total strain amplitude curves for the three alloys.

Table 6. Low cycle fatigue properties.

Alloy	σ'_f (MPa)	b	ε'_f	c
AA6005	488	-0.07	4.71	-1.04
AA6063	450	-0.09	3.92	-1.08
AA6351	470	-0.06	0.62	-0.90

with no stress amplitude reduction, which is associated with the presence of coarse particles α-(Fe,Mn)SiAl[30]. According to Molent et al.[31], Merati[32], such large particles are preferred for crack nucleation, thus explaining the low fatigue life for AA6063. The smaller size and more distributed particles in AA6005 and AA6351 the larger deviations of crack propagation and justifies the longer fatigue life.

Figure 8 shows the microstructure of AA6063 containing particles of α-(Fe,Mn)SiAl along the grain boundaries and etched with $K_4[Fe(CN)_6]$ and NaOH.

Figure 9 displays the *internal stress analysis* that considered friction stress, back stress, and peak stress obtained from hysteresis loop during 0.5% strain amplitude. A higher value of peak and friction stress rather than back stress is

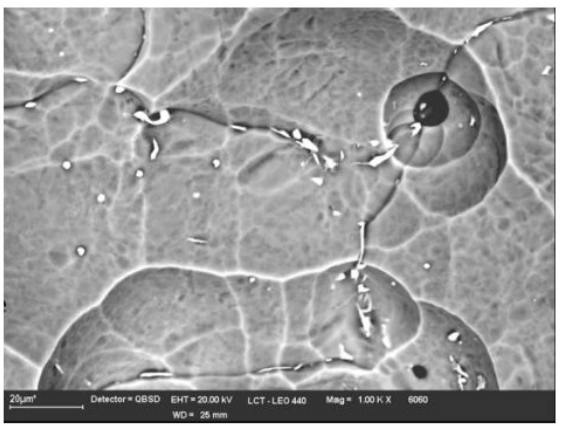

Figure 8. Microstructure of AA6063 (1000x magnification) by SEM[33].

observed for all alloys studied. Moreover, the friction stress is descending in the first stage and then reaches a steady state.

On the other hand, the back stress is ascending in the first stage of the test. AA6351 showed the highest friction stress values, whereas AA6063 showed lower values and

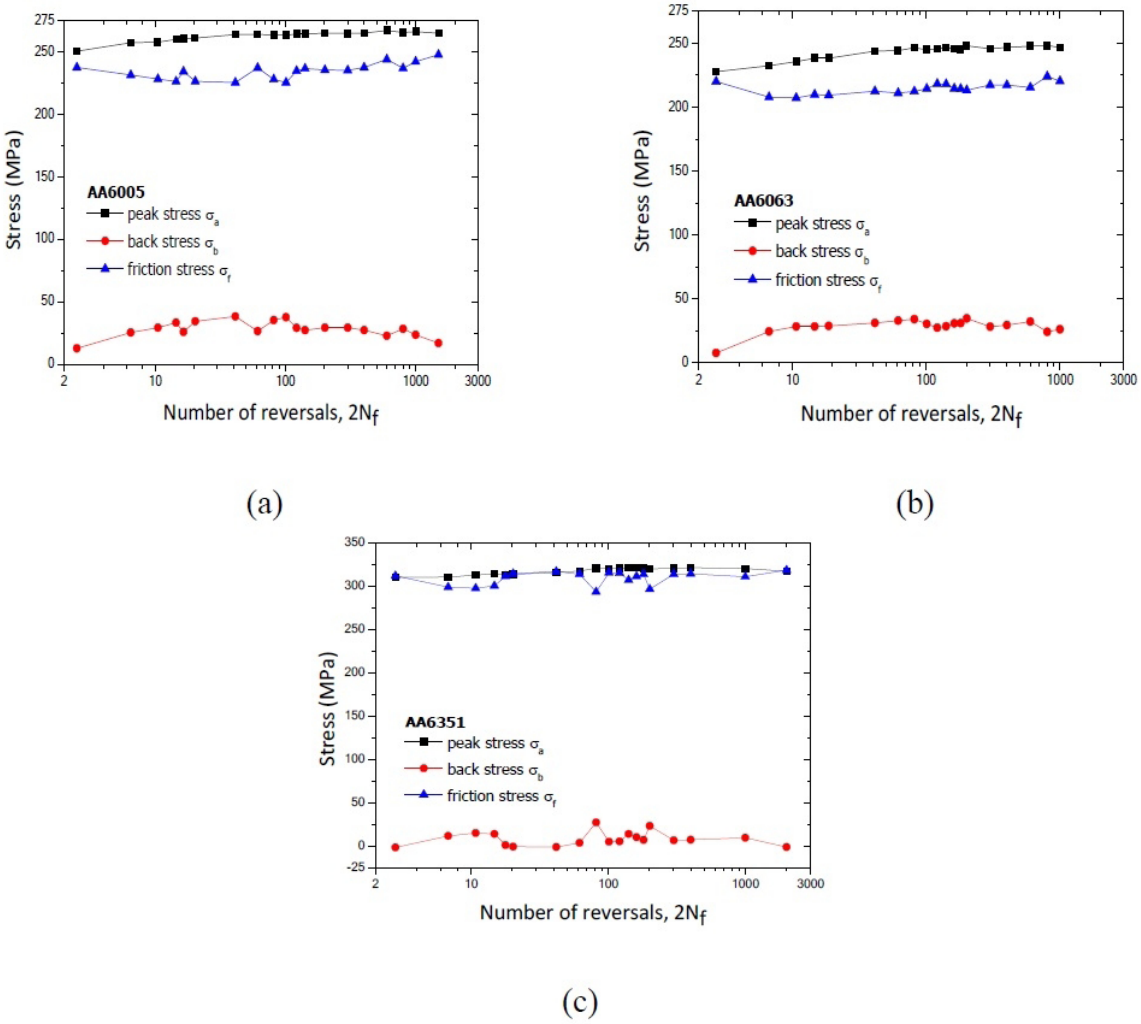

Figure 9. Evolution of internal stresses along cyclic strain. (a) AA6005, (b) AA6063, and (c) AA6351 (ε_a=0,5%).

a steady behavior for all internal stresses measured mainly due to coarse (Fe,Mn)SiAl and Mg_2Si particles.

The higher friction stress values of AA6351 are justified by high amount of intermetallic particles; consequently, during cyclic strain, the precipitates substantially contribute to the strain mechanism.

Table 7 shows the back-to-friction stress ratio for studied alloys. Despite the arbitrariness due to the definition of yield stress, it can be seen that AA6351 showed a lower back stress to friction stress ratio when compared to the other alloys. Plumtree and Abdel-Raouf[34], state a low back-to-friction stress ratio occurs when interparticle spacing is small and deformation is controlled by particles. Higher back-to-friction ratio indicates large interparticle spacing and deformation controlled by matrix.

Table 7. Back-to-friction stress ratio[34].

Alloy	σ_f [MPa]	σ_b [MPa]	σ_b / σ_f
AA6005	234	28	0.12
AA6063	215	28	0.13
AA6351	309	11	0.04

3.3.1. Effect of intermetallic phases on fatigue properties

Briefly, it is possible to summarize the effects of intermetallic phases and their distribution in main mechanical properties during fatigue tests according to Table 8. Again, as depicted in Table 4 the arrows show the trend of mechanical property influenced by intermetallic phase and its distribution. The discussion of results, were discussed in the previous topic.

Figure 10 depicts the *fractographic analysis* for (a) AA6005, (b) AA6063, and (c) AA6351. The striation spacing is 1-1.5μm in AA6351, approximately 3μm in AA6005, and 4μm in AA6063. The lowest striation spacing shown by AA6351 indicates its lower crack propagation rate compared to the other alloys. It also implies in high strength to crack propagation for AA6351 due

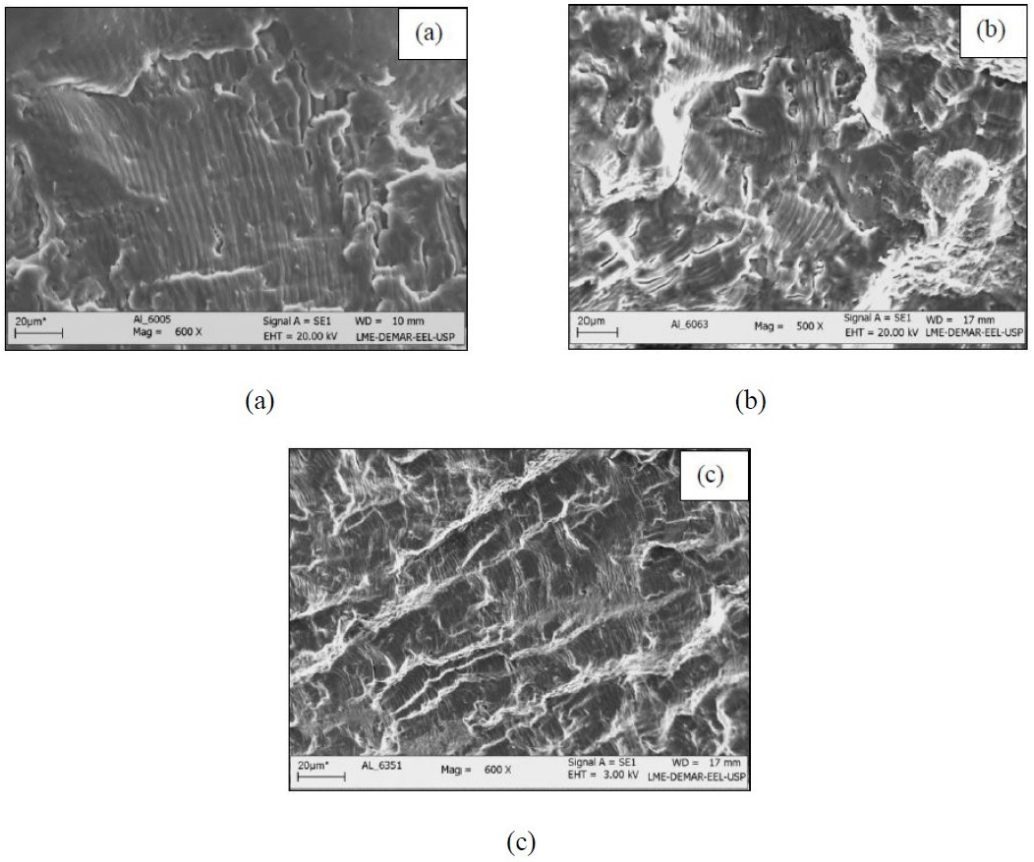

Figure 10. Fractography analysis showing striation for all alloys tested. (a) AA6005, (b) AA6063, and (c) AA6351.

Table 8. Intermetallic phases and their distribution effects.

Intermetallic phases and distribution	*n'*	*K'*	σ'f	ε'f	σ_f	σ_b	σ_b / σ_f
(Fe,Mn)SiAl	↑	-	↓	↓	↑	↓	-
Mg_2Si	↑	-	-	-	↑	↓	-
Large intermetallic spacing	-	-	-	-	-	-	↑
Small Intermetallic spacing	-	-	-	-	-	-	↓
Cause	*Low values associated to high SFE.*	*Strongly dependent alloy elements and hampering of dislocations*	*Large particles reduces fatigue lige, e. g. AA6063 alloy.*	*Large particles takes to premature fatigue*	*High amount of fine intermetallic phase*	*Large and coarse (FeMn)SiAl*	*Deformation controlled by matrix or precipitates*

to the short distance between precipitates, which changes the crack propagation way and increases the fatigue strength.

4. Conclusions

The results from tensile and fatigue tests correlated the mechanical behavior among alloys considering chemical composition, grain size, intermetallic size and distribution.

AA6351 showed the best mechanical properties in tensile tests, higher σ_{uts}, σ_y, E and lower ΔL, justified by the high amount of silicon and manganese, which contribute to the formation of hardener precipitates.

The AA6063 macrostructure showed a smaller and homogeneous grain size, however, the lowest fatigue strength due to the low amount of alloy elements. In fact, the presence of large intermetallic phases works as crack concentrators, thus reducing its fatigue life.

During low cycle behavior, AA6351 showed a low fatigue life for reversals lower than 1000 cycles mainly due to its low ductility. However, as the strain amplitude decreases,

the fatigue life increases for AA6351 alloy justified for showing a low σ_{uts} / σ_y ratio, and a low strain-hardening exponent implying in higher tolerance to fatigue damage. AA6063 showed lower strain-hardening exponent and σ_{uts} / σ_y ratio higher than those for other alloys resulting in the lowest fatigue life for low strain amplitudes.

Yet, for cyclic loading under strain control, AA6005 showed the highest fatigue strength coefficient (σ'_f) and the highest fatigue ductility coefficient (ε'_f). AA6063 showed the lowest fatigue strength coefficient (σ'_f) mainly due to the presence of coarse particles α-(Fe,Mn)SiAl that are preferred for crack nucleation, thus explaining the low fatigue life. AA6351 showed the lowest fatigue ductility coefficient (ε'_f) mainly due to the highest cyclic strain hardening exponent (n').

The highest value of friction stress for AA6351 indicates the effect of hardener precipitates as the most relevant role for cyclic strain control. On the other hand, AA6063 and AA6005 have shown the lower values of internal stresses due to their low amount of manganese and silicon.

The internal stress analysis also considers the back-to-friction stress ratio, and the lower value presented by AA6351 alloy indicates a lower interparticle spacing in this alloy, which plays a major role in the deformation behavior.

In short, the intermetallic phase analysis for tensile tests presents the $MnAl_6$ compound responsible for hampering of dislocations and promoting the hardening phenomena besides, the hardening effect of manganese and silicon as alloying elements. For fatigue tests analysis, the presence of large (FeMn) SiAl particles takes the material to premature fracture. Considering the internal stress analysis, friction stress is strongly affected by high amount of fine (FeMn) SiAl and Mg_2Si intermetallic particles. On the other hand, the back stress is affected by large and coarse (FeMn) SiAl and Mg_2Si particles. The back-to-friction stress ratio is very dependent of distance between particles.

5. Acknowledgments

The authors acknowledge the Coordination of Superior Level Staff Improvement (CAPES), Companhia Brasileira de Alumínio for material donation and C.A.R.P. Baptista is indebted to the National Council for Scientific and Technological Development (CNPq) for the research grants

6. References

1. Totten GE, Mackenzie DS. Handbook of aluminum. Abingdon: Routledge Taylor & Francis Group; 2003. Vol. 1, p. 169-72.
2. ASM International. Aluminum: properties and physical metallurgy. Materials Park, Ohio: ASM International; 1984.
3. ASM International. ASM International Handbook. Properties and Selection: nonferrous alloys and special purpose materials. 9th ed. Materials Park, Ohio: ASM International; 1990. Vol. 2.
4. Polmear IJ. Light alloys: metallurgy of the light metals. London: Edward Arnold; 1981.
5. Dumont D, Deschamps A, Brechet Y. On the relationship between microstructure, strength and toughness in AA7050 aluminum alloy. Mater Sci Eng A. 2003;A356(1-2):326-36. http://dx.doi.org/10.1016/S0921-5093(03)00145-X.
6. Azzam D, Menzemer CC, Srivatsan TS. The fracture behavior of an Al-Mg-Si alloy during cyclic fatigue. Mater Sci Eng A. 2010;527(20):5341-5.
7. Jiang X, He G, Liu B, Fan S, Zhu M. Microstructure based analysis fatigue behavior of Al-Si-Mg alloy. Trans Nonferrous Met Soc China. 2011;21(3):443-8. http://dx.doi.org/10.1016/S1003-6326(11)60734-6.
8. Dowling EM. Mechanical behavior of materials: engineering methods for deformation, fracture and fatigue. 3rd ed. New Jersey: Prentice Hall; 2007.
9. Lee Y-L, Pan J, Hathaway R, Barkey M. Fatigue Testing and Analysis. USA: Elsevier Inc.; 2005.
10. Chen X, Mørtsell EA, Sunde JK, O M, Marioara CD, Holmestad R, et al. Enhanced mechanical properties in 6082 aluminum alloy processed by cyclic deformation. Metals (Basel). 2021;11(11):1735. http://dx.doi.org/10.3390/met11111735.
11. Jain M. Evolution of internal stress variables during cyclic deformation of copper. Mater Sci Eng A. 1990;128(2):183-93. http://dx.doi.org/10.1016/0921-5093(90)90226-S.
12. Xu H, Ye D, Mei L. A study of the back stress and the friction stress behaviors of Ti-6Al-4V alloy during low cycle fatigue at room temperature. Mater Sci Eng A. 2017;700:530-9. http://dx.doi.org/10.1016/j.msea.2017.06.051.
13. Kuhlmann-Wilsdorf D, Laird C. Dislocation behavior in fatigue II: friction stress and back stress as inferred from an analysis of hysteresis loops. Mater Sci Eng. 1979;37(2):111-20. http://dx.doi.org/10.1016/0025-5416(79)90074-0.
14. Feaugas X, Clavel M. Cyclic deformation behavior of an α/β titanium alloy I: micromechanisms of plasticity under various loadings paths. Acta Mater. 1997;45(7):2685-701. http://dx.doi.org/10.1016/S1359-6454(96)00406-5.
15. Giordana M, Alvarez-Armas I, Armas A. Microstructural characterization of EUROFER 97 during low-cycle fatigue. J Nucl Mater. 2012;424(1-3):247-51. http://dx.doi.org/10.1016/j.jnucmat.2012.03.019.
16. Meininger JM, Gibeling JC. Low-cycle fatigue of niobium and niobium- 1Pct zirconium alloys. Metall Trans, A, Phys Metall Mater Sci. 1992;23A(11):3077-84. http://dx.doi.org/10.1007/BF02646126.
17. Proudhon H, Poole WJ, Wang X, Bréchet Y. The role of internal stresses on the plastic deformation of the Al–Mg–Si–Cu alloy AA6111. Philos Mag. 2008;88(5):621-40. http://dx.doi.org/10.1080/14786430801894569.
18. Bai C, Lan L, Xin R, Gao S, He B. Microstructure evolution and cyclic deformation behavior of Ti-6Al-4 V alloy via electron beam melting during low cycle fatigue. Int J Fatigue. 2022;159:106784. http://dx.doi.org/10.1016/j.ijfatigue.2022.106784.
19. American Society for Testing and Materials. E8/E8M-13 - Standard Test Methods for Tension Testing of Metallic Materials. West Conshohocken: ASTM; 2013.
20. American Society for Testing and Materials. E606/E606M-21 - Standard Test Method for Strain-Controlled Fatigue Testing. West Conshohocken: ASTM; 2021.
21. American Society for Testing and Materials. B221-21 - Standard Specification for Aluminum and Aluminum-Alloy Extruded Bars, Rods, Wire, Profiles, and Tubes. West Conshohocken: ASTM; 2021.
22. Cottrell AH. Dislocations and plastic flow in crystals. 3rd ed. London: Oxford University Press; 1965.
23. Nanninga N, White CL, Mills OP, Lukowski JT. Effect of specimen orientation and extrusion welds on the fatigue life of an AA6063 alloy. Int J Fatigue. 2009;32(2):238-46. http://dx.doi.org/10.1016/j.ijfatigue.2009.06.004.
24. Mrówka-Nowotnik G, Sieniawsky J. Influence of heat treatment on the microstructure and mechanical properties of 6005 and 6082 aluminum alloys. J Mater Charact. 2005;58:312-7.

25. Nam SW, Lee DH. The effect of Mn on the mechanical behavior of Al alloys. Met Mater. 2000;6(1):13-6. http://dx.doi.org/10.1007/BF03026339.
26. Borrego LP, Abreu LM, Costa JM, Ferreira JM. Analyses of low cycle fatigue in AlMgSi aluminum alloy. Eng Fail Anal. 2004;11(5):715-25. http://dx.doi.org/10.1016/j.engfailanal.2003.09.003.
27. Christ HJ, Mughrabi H. Cyclic stress-strain response and microstructure under variable amplitude loading. Fatigue Fract Eng Mater Struct. 1996;19(2-3):335-48. http://dx.doi.org/10.1111/j.1460-2695.1996.tb00971.x.
28. Liu X, He G, Ding X, Mo D, Zhang W. Fatigue behavior and dislocation substructures for 6063 aluminum alloy under nonproportional loadings. Int J Fatigue. 2009;31(7):1190-5. http://dx.doi.org/10.1016/j.ijfatigue.2008.11.019.
29. Brammer AT, Jordon JB, Allison PG, Barkey ME. Strain controlled low cycle fatigue properties of extruded 6061-T6 aluminum alloy. J Mater Eng Perform. 2013;22(5):1348-50. http://dx.doi.org/10.1007/s11665-012-0411-0.
30. Onurlu S, Tekin A. Effect of heat treatment on the insoluble intermetallic phases present in an AA 6063 alloy. J Mater Sci. 1994;29(6):1652-5. http://dx.doi.org/10.1007/BF00368940.
31. Molent L, Barter SA, Wanhill RJH. The lead crack fatigue-lifting framework. Netherlands: Department of defense, Defense Science and Technology Organization, Australian Government; 2010.
32. Merati A. A study of nucleation and fatigue behavior of an aerospace aluminum alloy 2024-T3. Int J Fatigue. 2005;27(1):33-44.
33. Borodiak M, Pinheiro FP, Paes M. Metallurgical characterization of aluminum alloys by matrix dissolution. In: Suarez CE, editor. Light metals 2012. Pittsburgh, PA: The Minerals, Metals & Materials Society; 2012. p. 455-60.
34. Plumtree A, Abdel-Raouf HA. Cyclic stress-strain response and substructure. Int J Fatigue. 2011;23(9):799-805. http://dx.doi.org/10.1016/S0142-1123(01)00037-8.